Since January 2020 Elsevier has created a COVID-19 resource centre with free information in English and Mandarin on the novel coronavirus COVID-19. The COVID-19 resource centre is hosted on Elsevier Connect, the company's public news and information website.

Free Radical Biology & Medicine 48 (2010) 704–712

Contents lists available at ScienceDirect

Free Radical Biology & Medicine

journal homepage: www.elsevier.com/locate/freeradbiomed

Original Contribution

Tempol ameliorates murine viral encephalomyelitis by preserving the blood–brain barrier, reducing viral load, and lessening inflammation

Maria Heloisa Tsuhako [a,*], Ohara Augusto [b,*], Edlaine Linares [b], Gerson Chadi [c], Selma Giorgio [d], Carlos A. Pereira [a]

[a] Laboratório de Imunologia Viral, Instituto Butantan, 05503-900 São Paulo, Brazil
[b] Instituto de Química, Departamento de Bioquímica, Department of Neurology, School of Medicine, Universidade de São Paulo, 05513-970 São Paulo, Brazil
[c] Neuroregeneration Center, Department of Neurology, School of Medicine, Universidade de São Paulo, 05513-970 São Paulo, Brazil
[d] Departamento de Biologia Animal, Instituto de Biologia, Universidade Estadual de Campinas, Campinas, Brazil

ARTICLE INFO

Article history:
Received 25 August 2009
Revised 9 December 2009
Accepted 16 December 2009
Available online 24 December 2009

Keywords:
Multiple sclerosis
Encephalomyelitis
Mouse hepatitis virus
Tempol
Antioxidant
Anti-inflammatory
Inflammation
Redox status
Nitric oxide-derived oxidants
Free radicals

ABSTRACT

Multiple sclerosis (MS) is a progressive inflammatory and/or demyelinating disease of the human central nervous system (CNS). Most of the knowledge about the pathogenesis of MS has been derived from murine models, such as experimental autoimmune encephalomyelitis and viral encephalomyelitis. Here, we infected female C57BL/6 mice with a neurotropic strain of the mouse hepatitis virus (MHV-59A) to evaluate whether treatment with the multifunctional antioxidant tempol (4-hydroxy-2,2,6,6-tetramethyl-1-piperidinyloxy) affects the ensuing encephalomyelitis. In untreated animals, neurological symptoms developed quickly: 90% of infected mice died 10 days after virus inoculation and the few survivors presented neurological deficits. Treatment with tempol (24 mg/kg, ip, two doses on the first day and daily doses for 7 days plus 2 mM tempol in the drinking water ad libitum) profoundly altered the disease outcome: neurological symptoms were attenuated, mouse survival increased up to 70%, and half of the survivors behaved as normal mice. Not surprisingly, tempol substantially preserved the integrity of the CNS, including the blood–brain barrier. Furthermore, treatment with tempol decreased CNS viral titers, macrophage and T lymphocyte infiltration, and levels of markers of inflammation, such as expression of inducible nitric oxide synthase, transcription of tumor necrosis factor-α and interferon-γ, and protein nitration. The results indicate that tempol ameliorates murine viral encephalomyelitis by altering the redox status of the infectious environment that contributes to an attenuated CNS inflammatory response. Overall, our study supports the development of therapeutic strategies based on nitroxides to manage neuroinflammatory diseases, including MS.

Multiple sclerosis (MS) is a progressive inflammatory and/or demyelinating disease of the human central nervous system. With an incidence of 1 per 1000 individuals, MS is the most prominent chronic neurological disease of young adults in the moderate climate areas of the Northern and Southern Hemispheres [1]. While there is a clear genetic influence [2,3], complex diseases such as MS are likely to involve inherited arrays of genetic polymorphisms, each exerting a slight effect on disease establishment and progression [4]. Environmental factors are also recognized as contributors to MS. Although the view that infectious agents encountered early in life may prime or trigger the disease process that manifests later in life is widely supported, incontrovertible evidence for a direct viral or bacterial trigger of MS has yet to be provided [1,5–7]. Because of the relative inaccessibility and sensitivity of the human central nervous system (CNS), most of the knowledge about the pathogenesis of MS has been derived from experimental animal models, such as murine experimental autoimmune encephalomyelitis (EAE) and murine viral encephalomyelitis [1,6–8].

Although the triggers of MS remain under scrutiny, it is widely accepted that an immune-mediated inflammatory response induced by lymphocytes, macrophages, and microglia in the CNS participates in the pathogenesis of the disease [1,6–8]. The resulting inflammatory environment favors high rates of superoxide anion and nitric oxide formation through NADPH oxidase and inducible nitric oxide synthase (iNOS), respectively [9–11]. These primary radicals lead to species that are more reactive toward biomolecules, such as peroxynitrite, nitrogen dioxide, carbonate radical, and myeloperoxidase compound I. They, in turn, may propagate the inflammatory cascade and/or trigger degenerative cascades leading to nitro-oxidative damage of the neural tissue [9–11]. Accordingly, the

Abbreviations: BBB, blood–brain barrier; CNS, central nervous system; EAE, experimental autoimmune encephalomyelitis; IFN-γ, interferon-γ; MHV, mouse hepatitis virus; MS, multiple sclerosis; iNOS, inducible nitric oxide synthase; tempol, 4-hydroxy-2,2,6,6,-tetramethyl-1-piperidinyloxy; TNF-α, tumor necrosis factor-α.

* Corresponding authors. M.H. Tsuhako is to be contacted at fax: +55 11 37261505. O. Augusto, fax: +55 11 30912186.
E-mail addresses: mariaheloisa@butantan.gov.br (M.H. Tsuhako), oaugusto@iq.usp.br (O. Augusto).

0891-5849/$ – see front matter © 2009 Elsevier Inc. All rights reserved.
doi:10.1016/j.freeradbiomed.2009.12.013

presence of 3-nitrotyrosine residues in proteins, a marker of nitro-oxidative damage, has been consistently demonstrated in acute and chronic active MS lesions of animal models and human patients (see, for instance [8,12–14]).

A particularly effective compound for deactivating nitrogen dioxide, carbonate radical, and the enzyme myeloperoxidase is the cyclic nitroxide radical tempol (4-hydroxy-2,2,6,6-tetramethyl-1-piperidinyloxy) [15–23]. Under physiological conditions, the nitroxide tempol ($TPNO^{\bullet}$) acts as a multifunctional antioxidant because it reacts with diverse biological oxidants and reductants while being recycled through the oxammonium cation ($TPNO^{+}$) and hydroxylamine derivative (TPNOH), respectively. After several catalytic cycles, tempol is eventually consumed by recombination reactions with specific radicals, such as tyrosyl and thiyl radicals and/or metabolized [15,19,21,23]. These nearly catalytic antioxidant properties are likely to contribute to the efficiency of tempol in reducing tissue injury in animal models of inflammation (reviewed in Refs. [15,24]).

To the best of our knowledge, there are no peer-reviewed studies reporting the effects of tempol on animal models of MS, although a patent has been recently published (WO 2009/023707 A1). In this case, the described examples were obtained with the murine EAE model. Here we show a striking effect of tempol in ameliorating murine viral encephalomyelitis induced by a neurotropic strain of the mouse hepatitis virus (MHV-59A) [6,7,25,26]. By monitoring disease scores, mouse survival, CNS integrity, viral load, and markers of inflammation, we also provide mechanistic clues to the ameliorating action of tempol.

Experimental procedures

Materials

All reagents were purchased from Sigma, Merck, or Fisher and were analytical grade or better. All solutions were prepared with distilled water purified with a Barnstead Milli-Q system.

Virus

Strain A59 of coronavirus MHV (MHV-59A) was obtained from the Laboratoire de Virologie (Strasburg, France). The virus was propagated and plaque assayed on L929 cell cultures in modified Eagle's medium containing 10% fetal bovine serum at 37°C, as previously described [27].

Infection of mice and tempol treatment

SPF female C57BL/6 mice (5–6 weeks of age) were obtained from our animal facilities, and the experiments performed followed the approved animal guidelines (Committee of Animal Ethics, Instituto de Química, Universidade de São Paulo). The animals were intracranially inoculated (ic) into the left cerebral hemisphere with 20 μl of a solution containing the MHV-59A virus (500 pfu) diluted in phosphate-buffered saline (PBS) containing 0.75% bovine serum albumin (BSA) or with PBS plus BSA (control animals) [25,26,28]. The injection was located in the deep cortical layer of the parietal cortex close to the corpus callosum as verified by pilot experiments in thaw-mounted brain sections of animals injected with Evan's blue. Tempol (24 mg/kg) was administered intraperitoneally (ip) in two doses on the first day (5 min before and 2 h after MHV-A59 inoculation) and in daily doses for 7 days between 9:00 and 10:00 AM; these animals also received tempol (2 mM) in the drinking water ad libitum [15,29]. Untreated animals were those that were inoculated with the virus and received PBS ip instead of tempol. Sham animals were those that received PBS plus BSA intracranially instead of the virus and were not treated with tempol.

Clinical features of infected mice

Mice were examined for clinical symptoms and scored as previously described [26]. In summary, normal mice scored 0; mildly sick animals (showing piloerection, hunched posture, and lethargy) scored 1; moderately sick mice (showing hind- or fore-limb weakness/paresis, lethargy) scored 2; severely sick animals (hind- or fore-limb paralysis, lethargy, depletion, ataxic gait) scored 3; moribund mice scored 4; and dead animals scored 5. Mice were euthanized with a lethal dose of thiopental (ip) for the collection of tissue samples and to interrupt the experiment.

Histopathologic analysis

At day 7 after infection, mice were euthanized with a lethal dose of thiopental (ip) and perfused intracardially with 10 ml of 10% buffered formalin. The brains were removed, formalin-fixed, paraffin-embedded, and stained with hematoxylin and eosin, to evaluate infiltration, and using Weil for demyelination assessment [30].

Viral titration

Mouse brain and spinal cord tissues were collected, weighed, and homogenized in DMEM supplemented with 10% fetal bovine serum and 50 μg/ml gentamycin. The homogenates (10–100 mg/ml) were serially diluted and plaque assayed on L929 cells [27].

Analysis of tempol and its hydroxylamine derivative by electron paramagnetic resonance (EPR)

EPR spectra were recorded at room temperature on a Bruker ER 200 D-SRC upgraded to an EMX instrument. Mice were sacrificed 10, 15, and 25 min after tempol administration (24 mg/kg; ip). Brain tissues were collected, homogenized in PBS (1.5 ml/g tissue), and subjected to EPR analysis before (to determine tempol levels) and after addition of 1 mM ferricyanide (to determine tempol plus hydroxylamine levels) [29]. The tempol concentration in the brain was estimated by double integration of the EPR spectrum and comparison with that of a standard tempol solution scanned under the same conditions. To determine the levels of tempol in the brain of animals receiving 2 mM tempol in the drinking water, the animals were sacrificed between 9:00 and 10:00 AM and the brain tissues were collected, homogenized, and analyzed by EPR as described above [29].

Determination of blood–CNS barrier permeability

Sodium fluorescein was used as a tracer as previously described with some modifications [31]. Briefly, mice received 100 μl of 10% sodium fluorescein in PBS ip and, 10 min later, were anesthetized, bled, and transcardially perfused with a minimum of 30 ml of PBS/heparin (1000 units/L) and PBS. Blood, brain, and spinal cords were collected for further analysis. The brains were washed with PBS and photographed. The spinal cords were weighed and homogenized in PBS (0.5 ml/spinal cord) and centrifuged (14,000 *g*, 2 min). A sample of the clarified supernatant was used to determine total protein concentration with a Bio-Rad kit. In parallel, 0.3 ml of the clarified supernatant was mixed with 1 ml of 15% trichloroacetic acid and centrifuged (10,000 *g*, 10 min). After the addition of 0.125 ml of 5 M NaOH to 0.5 ml of the supernatant, the fluorescence was determined by using a Fluorolog fluorimeter (SPEX) at 437 nm excitation and 508 nm emission. Sodium fluorescein standards (50–1000 ng/ml) were used to determine fluorescein contents in the samples. Blood was centrifuged and the levels of fluorescein in the sera were determined as above. Fluorescein uptake from the circulation into the spinal cord tissue is expressed as (μg fluorescence spinal cord tissue/

mg protein)/(μg fluorescence sera/μl blood) to normalize values for blood levels of the marker [31].

Immunohistochemical analysis

At 7 days after infection, mice were euthanized with a lethal dose of thiopental (ip) and perfused intracardially via the left ventricle with 20 ml of PBS followed by 20 ml of 10% buffered formalin. Brains and spinal cords were removed and kept in 10% buffered formalin (16–18 h). Tissue sections were paraffin-embedded and coronal sections (3 μm) were obtained and affixed onto slides. The slides were sequentially deparaffinized, rehydrated, and treated with 3% hydrogen peroxide for 10 min to block endogenous peroxidase activity. Then, the antigens were retrieved by incubating the slides at 100°C with citrate buffer, pH 6.0, for 1 min in a pressure cooker (in the case of anti-nitrotyrosine and Mac-2) or with Tris–EDTA buffer, pH 8.0, for 1 min in a vegetable steamer (for anti-iNOS). Finally, the slides were incubated at 4°C overnight with primary antibodies diluted in PBS/0.1% BSA. The employed antibodies and dilutions were mouse monoclonal to nitrotyrosine (Abcam, UK; 1:400), rabbit polyclonal to iNOS (Abcam; 1:1500), and monoclonal anti-mouse Mac-2 (Cedarlane, Canada; 1:50,000). After extensive washing with 0.5% TBS–Tween, the sections were incubated at 37°C in a humidified chamber with Novolink Max Polymer (Novocastra, UK) according to the instructions of the manufacturer for anti-nitrotyrosine and anti-iNOS antibodies. In the case of Mac-2 antibody, the sections were incubated with avidin biotinylated peroxidase complex (ABC), using the ABC Vectastain Elite kit (Vector Laboratories, Burlingame, CA, USA; 1:200) according to the instructions of the manufacturer. The avidin–biotin complex was visualized with 3,3′-diaminobenzidine (Sigma, St. Louis, MO, USA) and hydrogen peroxide. Counterstaining was performed with Harris's hematoxylin (Merck, Darmstadt, Germany). To assess nonspecific staining, the samples were similarly treated, but in the absence of the primary antibodies.

Morphometric/microdensitometric image analysis of immunoreactive brain sections

The Mac-2 (marker of macrophage cells), iNOS, and 3-nitrotyrosine immunoreactivity was measured in regions of the forebrain by semiquantitative bilateral image analysis (two sections/mouse; three animals) implemented on a Kontron–Zeiss KS400 image analyzer (Germany) as previously described [32]. Briefly, a television camera from the microscope acquired the image. The fields were selected within the brain regions of cortical areas, amygdaloid nuclei, hippocampus, and corpus callosum, bilaterally. The size of the sampled fields was 8.96×10^4 μm^2 (40×) for cortical areas, amygdaloid nuclei, and hippocampus and 1.21×10^4 μm^2 (63×) for corpus callosum. After shading correction, the following discrimination procedure was performed. The mean value of the gray matter (MGV ± standard error) in areas of the brain devoid of specific labeling was taken as the background. Gray values darker than the background were considered to correspond to specific labeling and discriminated. The specific MGV was taken as the difference between the specific and the background values. The glass value was left constant at 200 MGV. The morphometric (area) and the microdensitometric measurements (specific MGV) indicate the amount of immunopositive profiles in the sampled fields. Only the area of immunolabeling was presented.

Analysis of protein nitration by immune slot blot

At 7 days after infection, mice were euthanized with a lethal dose of thiopental (ip) and the spinal cord tissues were collected and immediately frozen in liquid nitrogen. The frozen tissues were pulverized with a pestle and mortar containing liquid nitrogen. Then, they were homogenized at 4°C with lysis buffer (0.18 ml/spinal cord) containing 50 mM Tris (pH 7.4), 0.5% Triton X-100, 5 mM EDTA, protease inhibitors (10 μg/ml trypsin inhibitor, 1 mM sodium orthovanadate, 10 μg/ml benzamidine, and 5 μg/ml antipain hydrochloride), and protease inhibition cocktail for tissues (1/2500 v/v; Sigma). The homogenate was centrifuged at 4°C and 1000 *g* for 10 min and the supernatant was stored at −80°C until analysis of total protein and nitrated protein (protein 3-nitrotyrosine). Total protein in the samples was determined by the Bradford method with a Bio-Rad kit. Samples of spinal cord homogenates (0.5 μg) were transferred onto a nitrocellulose membrane by vacuum for slot blots. Assessment of blotted protein was performed by Ponceau S staining as previously described [33]. The destaining was done with distilled water, and the membrane was blocked with 5% nonfat dried milk (2 h) before exposure to primary antibody solution for 1 h (mouse monoclonal anti-nitrotyrosine, 1/1000; Abcam). Primary antibody was detected by 1 h incubation with secondary antibody (peroxidase-conjugated rabbit polyclonal to mouse IgG, 1/5000; Abcam). Slot blots were revealed with chemiluminescence reagents (Amersham), and relative quantification of 3-nitrotyrosine was performed by densitometry (ImageQuant version 5.2; Molecular Dynamics) [15,29].

Assessment of TNF-α, IFN-γ, CD4, and CD8 transcripts by RT-PCR analysis

Mice were euthanized at 1 and 7 days after infection (for CD4 and CD8 analysis) and at 7 days after infection (for TNF-α and IFN-γ analysis) with a lethal dose of thiopental (ip), and the spleens and/or spinal cords were immediately removed. Total RNA was extracted using Trizol reagent (Invitrogen), following the instructions of the manufacturer. RNA concentration was determined by UV spectroscopy at 260 nm. Total RNA was reverse transcribed into cDNA with the Super Script first-strand synthesis system for RT-PCR (Invitrogen), following the instructions of the manufacturer. Amplification of cDNA was performed according to the instructions of the manufacturer (PCR master mix; Promega) in a thermal cycler (MJ Research, PTC 200). The protocols for IFN-γ, TNF-α, CD4, CD8, and β-actin transcript detection were as follows: in the case of IFN-γ, pre-denaturation at 94°C for 4.5 min and cycles of denaturation at 94°C for 20 s, annealing at 58°C for 20 s, and extension at 72°C for 30 s (repeated for 35 cycles) and a final end extension of 1 min at 72°C; for TNF-α, pre-denaturation at 95°C for 4 min and cycles of denaturation at 95°C for 20 s, annealing at 56°C for 20 s, and extension at 72°C for 30 s (repeated for 34 cycles) and a final end extension of 1 min at 72°C; for CD4 and CD8, pre-denaturation at 95°C for 15 min and cycles of denaturation at 94°C for 30 s, annealing at 60°C for 36 s, and extension at 72°C for 60 s (repeated for 40 cycles); and for β-actin, pre-denaturation at 95°C for 3 min and cycles of denaturation at 94°C for 45 s, annealing at 60°C for 45 s, and extension at 75°C for 45 s (repeated for 33 cycles) and a final end extension of 1 min at 72°C. The following primers were used for PCR amplification: IFN-γ primer (up, 5′-GCTCTGAGACAATGAACGCT-3′, and down, 5′-AAAGAGATAATCTGGCTCTGC-3′, 227 bp) [34]; TNF-α primer (up, 5′-TCTCATCAGTTCTATGGCCC-3′, and down, 5′-GGGAG-TAGACAAGGTACAAC-3′, 212 bp) [35]; CD4 primer (up, 5′-TCCTTCCCACTCAACTTTGC-3′, and down, 5′-AAGCGAGACCTGGGG-TATCT-3′, 200 bp); CD8 primer (up, 5′-GCTCAGTCATCAGCAACTCG-3′, and down, 5′-ATCACAGGCGAAGTCCAATC-3′, 200 bp) [36]; and β-actin primer (up, 5′-TGGAATCCTGTGGCATCCATGAAAC-3′, and down, 5′-TAAAACGCAGCTCAGTAACAGTCCG-3′, 348 bp) [37]. PCR products were analyzed on 1.5% agarose gel and stained with ethidium bromide (0.5 μg/ml). Relative quantification of the transcripts was performed by densitometry (ImageQuant version 5.2; Molecular Dynamics).

Statistical analysis

Data are expressed as means ± standard error. The differences between experimental groups were examined using the unpaired *t* test.

Results

Effects of tempol on the evolution of MHV-59A-induced encephalomyelitis

The outcome of viral infections depends on a variety of factors, such as host age, sex, and genetics and virus strain, mutability, dose, and route of administration [6,25,26]. Thus, we started by examining the characteristics of the MHV-59A infection in our experimental settings. SPF female C57BL/6 mice ($n = 12$) received PBS (ip) as a surrogate for the ulterior tempol treatment and intracranial inoculation of MHV-59A (500 pfu) and were maintained under observation. One day after infection, 50% of the animals showed mild neurological symptoms, such as piloerection, hunched posture, and lethargy (score 1) (Fig. 1A). Between 2 and 4 days after inoculation, some mice improved, but at least 70% showed moderate to severe neurological symptoms, such as hind- or fore-limb weakness/paresis (score 2) or hind- or fore-limb paralysis and ataxic gait (score 3). Between 6 and 8 days after infection, 30% of the mice died. Ten days after inoculation, 90% of the mice had died, and the survivors still presented neurological symptoms that persisted up to 60 days (Fig. 1A). Histopathological analysis of brain tissues collected 7 days after inoculation showed massive inflammatory cellular infiltration throughout forebrain gray and white matter regions (Fig. 1B). Inflammatory foci that were accumulating increased amounts of infiltrating cells were evident in gray matter regions, such as neocortex, hippocampus, amygdala, and diencephalon, and also in white matter structures, such as the lateral regions of the corpus callosum, internal capsule, anterior commissure, and fornix. Moreover, perivenous cuffing was particularly seen in the white matter clusters, mainly associated with perivenular disruption of the myelin staining by Weil (Fig. 1B). Thus, we confirmed that MHV-A59 infection of SPF female C57BL/6 mice models certain of the aspects of the CNS inflammation associated with MS [5–7], being useful to test the effects of tempol treatment.

Functional and analytical studies have demonstrated that tempol penetrates the blood–brain barrier (reviewed in [38]). This was confirmed by EPR analysis of brain homogenates of sham and MHV-59A-infected mice sacrificed 10, 15, or 25 min after tempol administration (24 mg/kg; ip; Fig. 2). As is usual in biological fluids and tissues, most of the tempol was present in its reduced form, the corresponding hydroxylamine. Indeed, the characteristic EPR signal of tempol became noticeable upon addition of ferricyanide to the homogenates [29]. Total tempol (nitroxide plus hydroxylamine) levels decayed quickly in vivo, attaining about 0.3 μM in brain 25 min after administration. Maximum levels (about 15 μM) were measured 10 min after administration in sham mice. The lower levels

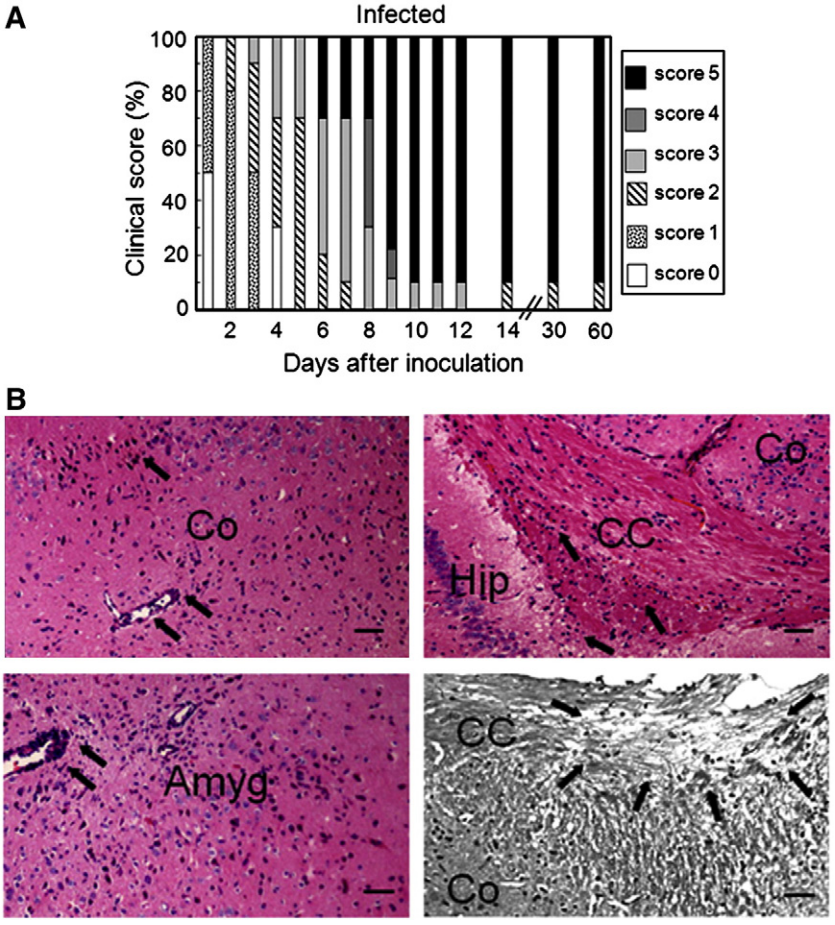

Fig. 1. (A) Evolution of clinical symptoms and (B) histology of brain tissues 7 days postinfection of female C57BL/6 mice infected with MHV-A59 (500 pfu; ic). Infection and analysis were performed as described under Experimental procedures. (A) Neurological symptoms of the mice ($n = 12$) were scored as described in the text and under Experimental procedures. In summary, scores 0, 1, 2, 3, 4, and 5 correspond to normal, mildly sick, moderately sick, severely sick, moribund, and dead mice, respectively. (B) Representative hematoxylin/eosin- and Weil-stained (bottom right) sections from brains of MHV-A59-infected mice 7 days postinfection. The regions are labeled as Co (cortical area), Amyg (amygdaloid nucleus), Hip (hippocampus), and CC (corpus callosum). Massive inflammatory cellular infiltration and loci of myelin disruption are marked by single and encircling arrows, respectively. Scale bars, 10 μm.

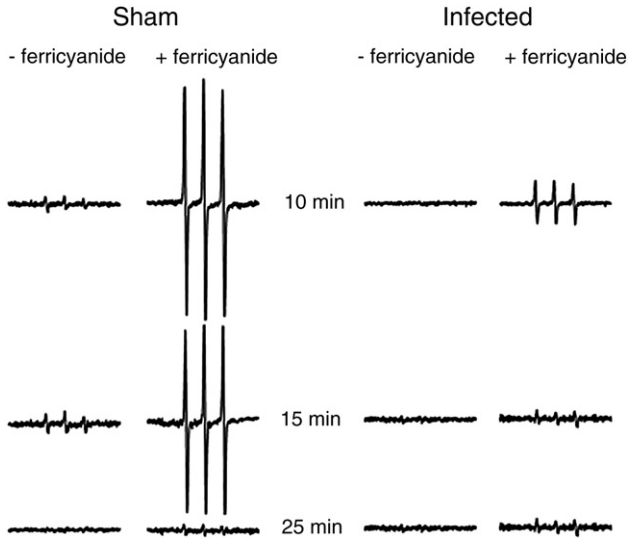

Fig. 2. Representative EPR spectra of brain homogenates of sham and MHV-59A-inoculated female C57BL/6 mice 1 day postinfection sacrificed at different times after tempol administration (24 mg/kg; ip). The spectrum of each homogenate was scanned before and after addition of 1 mM ferricyanide, as indicated. Instrument conditions: microwave power, 10 mW; modulation amplitude, 0.1 mT; time constant, 327 ms; scan rate, 0.029 mT/s.

of total tempol detected in infected mice (about 3 μM after 10 min) are consistent with the course of infection producing radicals that are able to react with tempol to generate redox inactive products [29].

Despite the fast metabolism of tempol in mice (Fig. 2), treatment of MHV-59A-infected mice with this compound profoundly altered the outcome of the disease. For example, the neurological symptoms and CNS infiltration and demyelination were greatly reduced (Fig. 3), and mouse survival was significantly increased (Fig. 4). Indeed, histopathological analysis of the forebrain regions of tempol-treated mice revealed a dramatic reduction in inflammatory cell infiltration throughout the forebrain gray and white matter regions. In addition, perivenous accumulation of inflammatory cells and disruption of the Weil's myelin stain were substantially reduced (compare Figs. 1B and 3B). Whereas 90% of untreated mice died at 10 days after infection, 70% of the mice treated with tempol survived (Fig. 4) and about half of them displayed the behavior of normal mice (Fig. 3A). These striking effects were obtained with tempol administration (24 mg/kg; ip) in two doses on the first day (5 min before and 2 h after MHV-A59 inoculation) and in daily doses for 7 days; the animals also received tempol (2 mM) in the drinking water ad libitum [29]. No adverse effects of this treatment were observed in uninfected mice (Fig. 4). Previously, we have shown that tempol administered in the drinking water was distributed to tissues but we did not examine CNS tissues [29]. Now, we determined the levels of total tempol (tempol plus hydroxylamine) in the brain, spinal cord, and plasma of mice receiving 2 mM tempol in the drinking water. These levels were similar and around 0.3 μM (data not shown).

The mechanisms by which tempol ameliorates viral encephalomyelitis

To gain insight into the mechanisms by which tempol ameliorates viral encephalomyelitis, we first examined whether the nitroxide

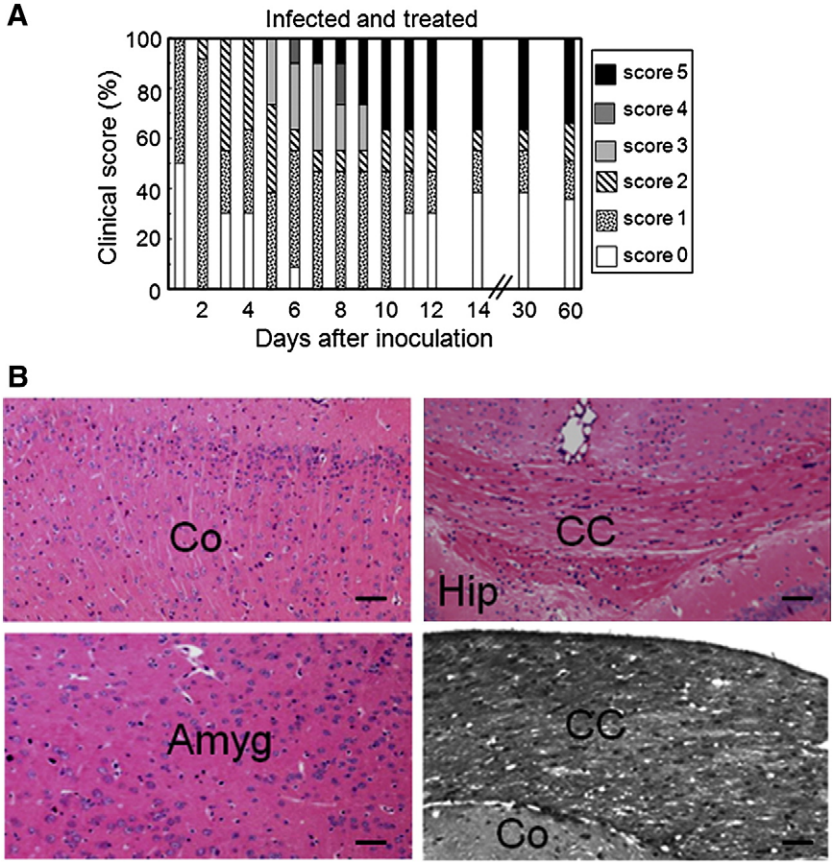

Fig. 3. (A) Evolution of clinical symptoms and (B) histology of brain tissues 7 days postinfection of female C57BL/6 mice infected with MHV-A59 (500 pfu; ic) and treated with tempol. Infection, treatment, and analysis were performed as described under Experimental procedures. (A) Neurological symptoms of the mice ($n = 12$) were scored as described for Fig. 1. (B) Representative hematoxylin/eosin- and Weil-stained (bottom right) sections from brains of MHV-A59-infected mice treated with tempol 7 days postinfection. The regions were labeled as Co (cortical area), Amyg (amygdaloid nucleus), Hip (hippocampus), and CC (corpus callosum). In contrast to the brains of untreated mice (Fig. 1B), massive inflammatory cellular infiltration and loci of myelin disruption are largely absent.

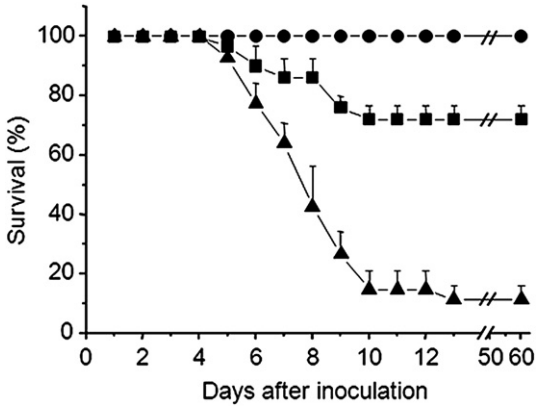

Fig. 4. Survival of female C57BL/6 mice inoculated with MHV-A59 and treated with tempol (■) or not treated (▲). Inoculation of MHV-A59 (500 pfu; ic) and treatment were performed as described under Experimental procedures. Control animals (●) were those that received PBS intracranially instead of the virus and were treated with tempol. The values shown correspond to the means ± standard error of five groups of animals ($n = 5$ or 6 each).

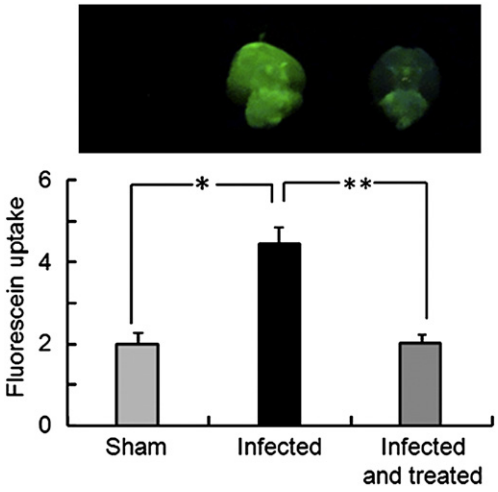

Fig. 5. Permeability of the BBB 7 days postinfection in female C57BL/6 mice inoculated with MHV-A59 and treated or not with tempol. Inoculation of MHV-A59 (500 pfu; ic), treatment, and measurement of BBB permeability were performed as described under Experimental procedures. Fluorescein uptake is expressed as (μg fluorescence spinal cord tissue/mg protein)/(μg fluorescence sera/μl blood). The values shown correspond to the means ± standard error of eight (control), seven (tempol-treated), and four (sham) mice; *$p<0.002$, **$p<0.0002$, unpaired t test. Representative photographs of brains are also shown for qualitative assessment of BBB permeability.

affected viral load in the CNS (Table 1). One day after inoculation, virus titers were undetectable by plaque assay in the CNS of both untreated and tempol-treated mice. By the time the first animals died, between 6 and 7 days after inoculation, virus titers were high in both the brain and the spinal cord of untreated mice but were significantly reduced in mice treated with tempol (Table 1).

Next, we examined blood–brain barrier (BBB) integrity because its loss has been associated with several neurological diseases, including MS [39]. To this end, the uptake of the fluid-phase marker sodium fluorescein was assessed quantitatively and qualitatively in the spinal cords and brains of mice, respectively. The results show that 7 days after MHV-59A inoculation there was a marked increase in the permeability of the BBB of untreated mice (Fig. 5). In contrast, tempol-treated animals presented a remarkably preserved BBB.

In addition to the loss of blood–brain barrier integrity, CNS inflammation is a crucial event in the pathogenesis of MS. Thus, we complemented the histopathological analysis of CNS tissues of MHV59A-infected mice (Figs. 1B and 3B) with immunohistochemical and RT-PCR analysis of markers of inflammation. Immunohistochemical analysis of the brain (Fig. 6) and spinal cord (data not shown) tissues showed that viral infection resulted in macrophage infiltration, iNOS expression, and protein nitration, all of which were greatly attenuated by tempol treatment. In some brain sections of infected mice, activated glial cells strongly staining for nitrated proteins were noticeable (Fig. 6, bottom left). Semiquantitative image analysis of the immunostaining of the brain tissues revealed that treatment with tempol reduced macrophage infiltration, iNOS expression, and 3-nitrotyrosine levels to about 4, 26, and 16% of those of untreated mice, respectively (Fig. 7A). Quantification of 3-nitrotyrosine levels in the spinal cords of the animals by immune slot blot confirmed that tempol inhibited its levels to about 12% of those of untreated mice (Fig. 7B). Treatment with tempol also greatly reduced the levels of TNF-α and IFN-γ mRNAs in the spinal cords of the animals as assessed by RT-PCR (Fig. 7C). These cytokines can be produced by T cells, which are involved in the immune and inflammatory response during viral encephalomyelitis [reviewed in 6,7]. Thus, we also quantified the levels of CD4 and CD8 mRNA in the spinal cords and spleens of the animals. Treatment with tempol decreased the infiltration of $CD4^+$ and $CD8^+$ T lymphocytes into the spinal cords, although only the differences in CD8 mRNA levels were statistically significant (Figs. 8A and 8C). Tempol did not alter the levels of CD4 and CD8 transcripts in the spleen (Fig. 8A), indicating a preserved immune status of the treated animals. Naive mice presented lower levels of CD4 and CD8 transcripts (Fig. 8B) than infected animals (Fig. 8A), as can be inferred from the relative intensity of the corresponding CD4, CD8, and β-actin bands. These results demonstrate that tempol strongly inhibited the CNS inflammation of MHV-59A-infected mice (Figs.1, 3, 6, and 7) without compromising their immune system (Fig. 8).

Table 1
Virus titers in the CNS of MHV-59A-infected female C57BL/6 mice treated or not with tempol 1 and 7 days postinfection (dpi)[a]

	Virus titer (log_{10}) (pfu/mg tissue)	
	1 dpi	7 dpi
Spinal cord*		
Untreated mice	ND[b]	4.2 ± 0.2[c]
Treated mice	ND	1.6 ± 0.3
Brain**		
Untreated mice	ND	4.4 ± 0.1
Treated mice	ND	0.8 ± 0.2

[a] Virus inoculation, animal treatment, and determination of titers were performed as described under Experimental procedures.
[b] Not detectable by plaque assay.
[c] The values correspond to the mean ± standard error of five (untreated) or three (tempol-treated) animals.
* $p<0.0004$ compared with untreated mice, unpaired t test.
** $p<0.0001$ compared with untreated mice, unpaired t test.

Discussion

The results reported here show that treatment with tempol is quite effective in ameliorating MHV-59A virus-induced murine encephalomyelitis. In our experimental setting, the neurological symptoms and CNS alterations developed quickly, and 90% of the mice died 10 days after virus inoculation (Figs. 1A and 4). Treatment with tempol attenuated these neurological symptoms and increased survival up to 70% (Figs. 3A and 4). Notably, half of the survivors behaved as normal mice, at least when kept at a low dose of tempol in the drinking water (2 mM). Not surprisingly, treatment with tempol substantially preserved the integrity of the CNS (compare Figs. 1B and 3B), including the BBB (Fig. 5).

The effects of tempol in preserving the neurological behavior and the CNS integrity of infected mice were accompanied by a pronounced reduction in the infiltration of macrophages and $CD8^+$ T

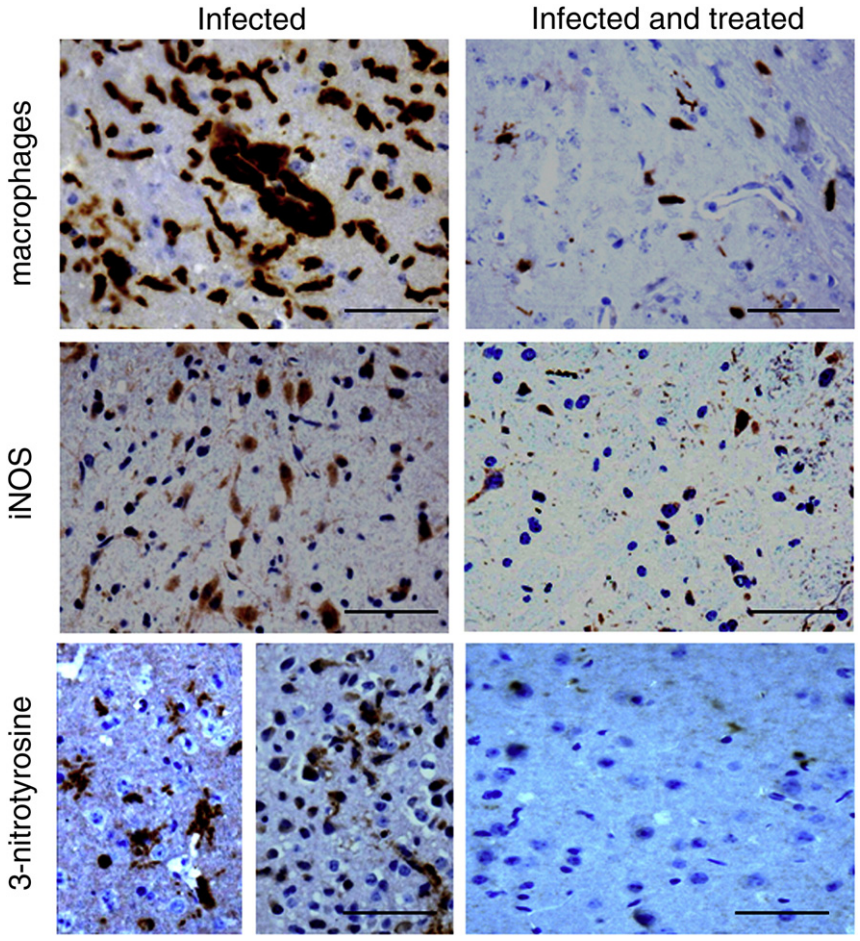

Fig. 6. Representative photomicrographs of brain sections 7 days postinfection of female C57BL/6 mice inoculated with MHV-A59 and treated or not with tempol. Sections were immunohistochemically stained using Mac-2, iNOS, and nitrotyrosine antibodies as specified. Sections were counterstained with Harris's hematoxylin. The procedures employed are described under Experimental procedures. Slides were examined with a 40× lens, photographed, and printed under the same conditions. Scale bars, 50 μm.

lymphocytes into the CNS (Figs. 6A, 7A, and 8). Systemic T cells did not decrease, excluding a major immunosuppressive effect of tempol (Fig. 8) [40]. Treatment with tempol also reduced the tissue levels of markers of inflammation, such as expression of iNOS, TNF-α and IFN-γ transcription, and protein nitration (Figs. 6 and 7). In these animals, the inhibition of protein nitration (about 86%) was higher than that of iNOS expression (about 74%; Figs. 7A and B), indicating that tempol is acting as both an antioxidant and a regulator of iNOS expression [29].

The antioxidant action of tempol during the MHV-59A virus-induced encephalomyelitis was also revealed by the faster decay rate of tempol plus hydroxylamine in the brains of infected mice compared with sham mice (Fig. 2). This indicates that the infectious process generates a considerable amount of radicals, some of which are able to react with tempol to produce redox-inactive products [29]. Consequently, tempol altered the redox status of the infectious environment (Fig. 2). On the other hand, it is being increasingly recognized that the redox status of extra- and intracellular microenvironments influences the outcome of infectious/inflammatory processes [41–43]. Thus, it is likely that tempol attenuated the CNS inflammatory response and ameliorated viral encephalomyelitis (Figs. 1 and 3–8) by altering the redox status of the infectious environment (Fig. 2). In this regard, our study supports the argument that the antioxidant and anti-inflammatory actions of tempol are likely to be interrelated [29,38,44].

The effects of tempol on redox signaling cascades involved in inflammatory processes, however, remain poorly investigated at the molecular level [38]. At the phenomenological level, tempol has been previously shown to display anti-inflammatory properties in mouse models of infectious/inflammatory diseases. For instance, tempol administration decreased the levels of TNF-α mRNA and inhibited NF-κB activation in mice subjected to carrageenan-induced pleuritis [44] and inhibited iNOS expression in murine leishmaniasis [29]. In the case of the MHV-59A-infected mice, treatment with tempol reduced the levels of iNOS protein (Figs. 6 and 7) and viral load into the CNS (Table 1). This reduction in viral load contrasts with our previous observation that in reducing iNOS expression and protein nitration in murine leishmaniasis, tempol increases parasite load in cutaneous lesions [29].

The opposite effects of nitric oxide-derived oxidants in different infectious diseases are likely to result from the diverse modes of microbial replication and invasion of host tissues [45,46]. In contrast with most bacteria and parasites, virus cannot be confined to limited areas by the nonspecific host defense mediated by phagocytes and their mediators. In consequence, nitric oxide-derived oxidants are more likely to cause nonspecific nitro-oxidative damage in virus-infected tissue than to eliminate the virus [47–49]. Accordingly, it has been reported that infection of iNOS knockout (−/−) and iNOS (+/+) mice with MHV resulted in similar kinetics of virus clearance, but in reduced neuronal apoptosis and mortality [50]. We did not follow the kinetics of virus clearance in our experimental setting, but we did show that 7 days after infection, tempol reduced viral load, iNOS expression, and CNS damage. Thus, it is feasible that by decreasing nitro-oxidative stress, tempol attenuates the mutation rate of the virus, precluding evolution of mutants able to escape the antiviral immune responses of the host [45,46]. Additionally, tempol

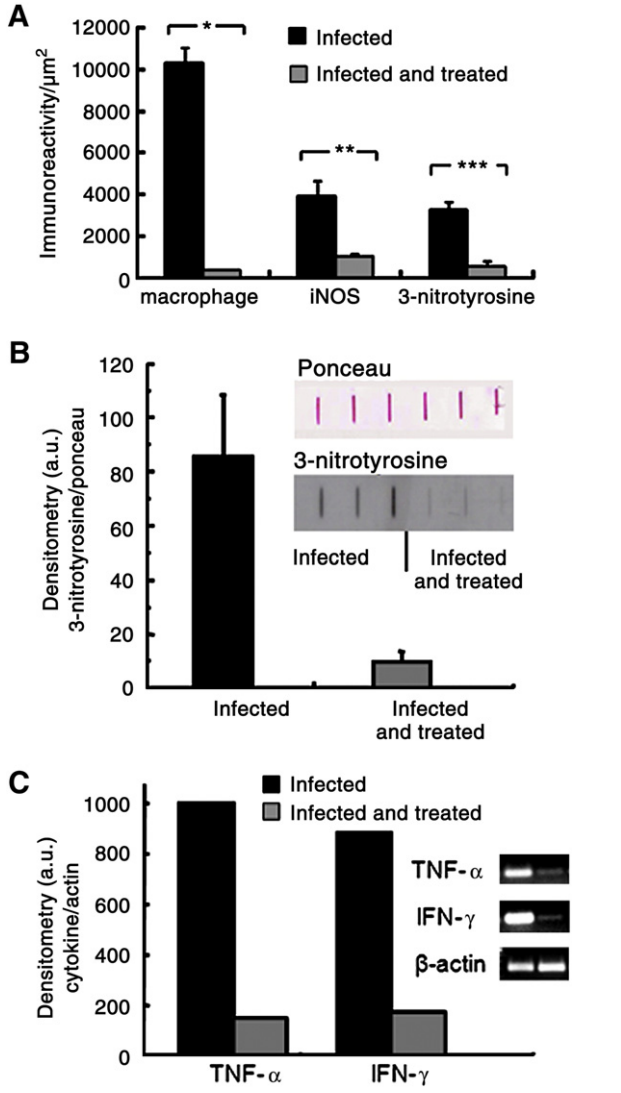

Fig. 7. Relative quantification of markers of inflammation in the CNS 7 days postinfection of female C57BL/6 mice inoculated with MHV-A59 and treated or not with tempol. Inoculation of MHV-A59 (500 pfu; ic), treatment, and analysis were performed as described under Experimental procedures. (A) Semiquantitative microdensitometric/morphometric image analysis of immunoreactive areas of Mac-2, iNOS, and 3-nitrotyrosine in the brain of the animals as specified. The data obtained in all analyzed regions were normalized in a sampled field of $8.96 \times 104\ \mu m^2$ and pooled together to be expressed. The values shown correspond to the means ± standard error ($n = 3$); *$p < 0.0002$, **$p < 0.02$, ***$p < 0.004$, unpaired t test. (B) Relative quantification of 3-nitrotyrosine in the spinal cord of the specified animals by immune slot blot. The values correspond to the means ± standard error ($n = 3$); $p < 0.03$, unpaired t test (not shown for clarity). The inset shows representative blots. (C) Relative quantification of TNF-α and IFN-γ transcripts in the spinal cords of the specified animals. The values correspond to the means of two independent experiments. The inset shows the results of one of the experiments.

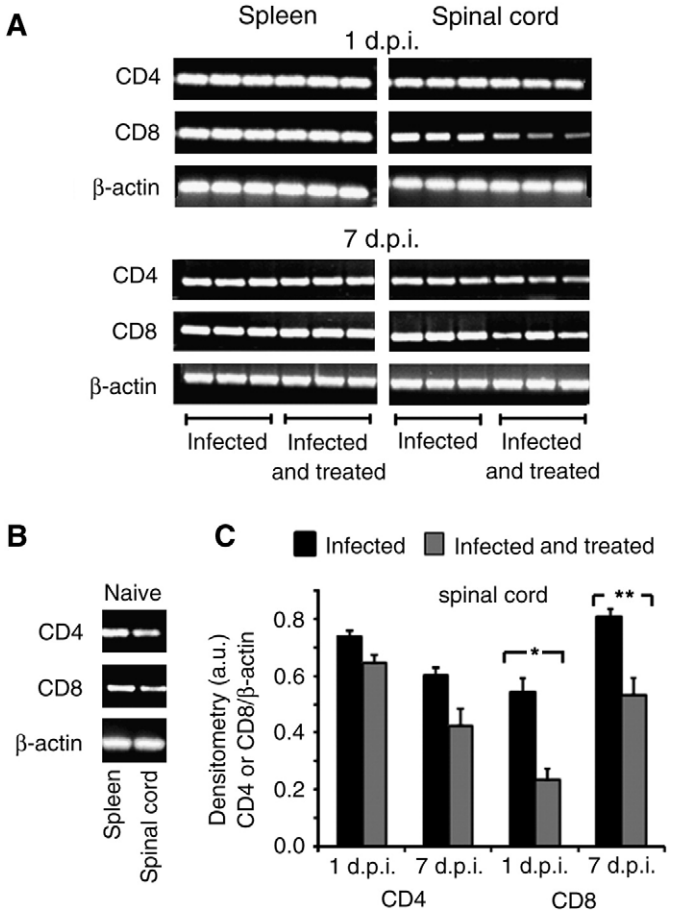

Fig. 8. Relative quantification of CD4 and CD8 mRNA in the spleen and spinal cord 1 and 7 days postinfection of female C57BL/6 mice inoculated with MHV-A59 and treated or not with tempol. Inoculation of MHV-A59 (500 pfu; ic), treatment, and analysis were performed as described under Experimental procedures. (A) Representative results obtained from three infected mice each, untreated or treated with tempol as specified. (B) Representative results obtained from naive mice. (C) Relative quantification of CD4 and CD8 transcripts in the spinal cords by densitometry of the corresponding bands shown in (A). The values correspond to the means ± standard error; *$p < 0.01$, **$p < 0.02$, unpaired t test.

may inhibit virus entrance into host cells by altering the redox state of the cells and of their surface proteins. Indeed, there are previous studies showing that viral infection and replication are dependent on the redox status of infectious microenvironments [41,42].

Taken together, our results indicate that tempol ameliorates murine viral encephalomyelitis by altering the redox status of the infectious environment that contributes to an attenuated CNS inflammatory response (Figs. 1 and 3–8). Thus, our study argues for the interrelatedness of the antioxidant and anti-inflammatory actions of tempol [29,38,44]. This cross talk, however, remains to be examined at the molecular level. With regard to therapeutic implications, it is important to note that the natural antioxidant uric acid has been shown to be quite effective in ameliorating EAE by inhibiting CNS inflammation, BBB dysfunction, and tissue damage [8,12,51,52]. This discovery motivated the initiation of clinical trials with inosine, a metabolic precursor of uric acid. Oral administration of inosine increases uric acid levels in both serum and cerebrospinal fluid, whereas an oral dose of uric acid is mostly degraded by uricase in the gastrointestinal tract. The ameliorating effects of uric acid in EAE have been attributed to its ability to scavenge nitric oxide-derived oxidants [8,12,51,52]. In comparison, tempol is more effective than uric acid in scavenging nitric oxide-derived oxidants [9], displays low toxicity in animal models [15,16], permeates the blood–brain barrier (Fig. 2), and inhibits the enzyme myeloperoxidase ([20]; see Augusto et al., [53], which has been recently associated with MS [54,55]. In this context, the reported ameliorating effects of tempol on viral murine encephalomyelitis provide support for the development of therapeutic strategies based on nitroxides to manage neuroinflammatory diseases, including MS.

Acknowledgments

This work was supported by grants from the Fundação de Amparo à Pesquisa do Estado de São Paulo (FAPESP) and Conselho Nacional de Desenvolvimento Científico e Tecnológico (CNPq). O.A. and E.L. are members of the INCT de Processos Redox em Biomedicina-Redoxoma (CNPq/FAPESP).

References

[1] 't Hart, B. A.; Hintzen, R. Q.; Laman, J. D. Multiple sclerosis—a response-to-damage model. *Trends Mol. Med.* **15:**235–244; 2009.

[2] Ebers, G. C.; Sadovnick, A. D.; Risch, N. J. Canadian Collaborative Study Group. A genetic basis for familial aggregation in multiple sclerosis. *Nature* **377:**150–151; 1995.

[3] International Multiple Sclerosis Genetics Consortium Risk alleles for multiple sclerosis identified by a genomewide study. *N. Engl. J. Med.* **357:**851–862; 2007.

[4] Risch, N.; Merikangas, K. The future of genetic studies of complex human diseases. *Science* **273:**1516–1517; 1996.

[5] Fazakerley, J. K.; Walker, R. Virus demyelination. *J. Neurovirol.* **9:**148–164; 2003.

[6] Lane, T. E.; Buchmeier, M. J. Murine coronavirus infection: a paradigm for virus-induced demyelinating disease. *Trends Microbiol.* **5:**9–14; 1997.

[7] Glass, W. G.; Chen, B. P.; Liu, M. T.; Lane, T. E. Mouse hepatitis virus infection of the central nervous system: chemokine-mediated regulation of host defense and disease. *Viral Immunol.* **15:**261–272; 2002.

[8] Gonsette, R. E. Neurodegeneration in multiple sclerosis: the role of oxidative stress and excitotoxicity. *J. Neurol. Sci.* **274:**48–53; 2008.

[9] Augusto, O.; Bonini, M. G.; Amanso, A. M.; Linares, E.; Santos, C. C.; de Menezes, S. L. Nitrogen dioxide and carbonate radical anion: two emerging radicals in biology. *Free Radic. Biol. Med.* **32:**841–859; 2002.

[10] Radi, R. Nitric oxide, oxidants, and protein tyrosine nitration. *Proc. Natl. Acad. Sci. USA* **101:**4003–4008; 2004.

[11] Szabó, C.; Ischiropoulos, H.; Radi, R. Peroxynitrite: biochemistry, pathophysiology and development of therapeutics. *Nat. Rev. Drug Discovery* **6:**662–680; 2007.

[12] Scott, G. S.; Spitsin, S. V.; Kean, R. B.; Mikheeva, T.; Koprowski, H.; Hooper, D. C. Therapeutic intervention in experimental allergic encephalomyelitis by administration of uric acid precursors. *Proc. Natl. Acad. Sci. USA* **99:**16303–16308; 2002.

[13] Teixeira, S. A.; Castro, G. M.; Papes, F.; Rogério, F.; Langone, F.; Santos, L. M.; Arruda, P.; de Nucci, G.; Muscará, M. N. Expression and activity of nitric oxide synthase isoforms in rat brain during the development of experimental allergic encephalomyelitis. *Brain Res. Mol. Brain Res.* **99:**17–25; 2002.

[14] Zeis, T.; Probst, A.; Steck, A. J.; Stadelmann, C.; Brück, W.; Schaeren-Wiemers, N. Molecular changes in white matter adjacent to an active demyelinating lesion in early multiple sclerosis. *Brain Pathol.* **19:**459–466; 2008.

[15] Augusto, O.; Trindade, D. F.; Linares, E.; Vaz, S. M. Cyclic nitroxides inhibit the toxicity of nitric oxide-derived oxidants: mechanisms and implications. *An. Acad. Bras. Cienc.* **80:**179–189; 2008.

[16] Soule, B. P.; Hyodo, F.; Matsumoto, K.; Simone, N. L.; Cook, J. A.; Krishna, M. C.; Mitchell, J. B. The chemistry and biology of nitroxide compounds. *Free Radic. Biol. Med.* **42:**1632–1650; 2007.

[17] Goldstein, S.; Samuni, A.; Hideg, K.; Merenyi, G. Structure–activity relationship of cyclic nitroxides as SOD mimics and scavengers of nitrogen dioxide and carbonate radicals. *J. Phys. Chem. A* **110:**3679–3685; 2006.

[18] Goldstein, S.; Samuni, A.; Merenyi, G. Reactions of nitric oxide, peroxynitrite and carbonate radical with nitroxides and their corresponding oxammonium cations. *Chem. Res. Toxicol.* **17:**250–257; 2004.

[19] Vaz, S. M.; Augusto, O. Inhibition of myeloperoxidase-mediated protein nitration by tempol: kinetics, mechanism, and implications. *Proc. Natl. Acad. Sci. USA* **105:** 8191–8196; 2008.

[20] Rees, M. D.; Bottle, S. E.; Fairfull-Smith, K. E.; Malle, E.; Whitelock, M.; Davies, M. J. Inhibition of myeloperoxidase-mediated hypochlorous acid production by nitroxides. *Biochem. J.* **421:**79–85; 2009.

[21] Goldstein, S.; Samuni, A.; Merenyi, G. Kinetics of the reaction between nitroxide and thiyl radicals: nitroxides as antioxidants in the presence of thiols. *J. Phys. Chem.* **112:**8600–8605; 2008.

[22] Lam, M. A.; Pattison, D. I.; Bottle, S. E.; Keddie, D. J.; Davies, M. J. Nitric oxide and nitroxides can act as efficient scavengers of protein-derived free radicals. *Chem. Res. Toxicol.* **21:**2111–2119; 2008.

[23] Borisenko, G. G.; Martin, I.; Zhao, Q.; Amoscato, A. A.; Kagan, V. E. Nitroxides scavenge myeloperoxidase-catalyzed thiyl radicals in model systems and in cells. *J. Am. Chem. Soc.* **126:**9221–9232; 2004.

[24] Thiemermann, C. Membrane-permeable radical scavengers (tempol) for shock, ischemia–reperfusion injury, and inflammation. *Crit. Care Med.* **31:**S76–S84; 2003.

[25] Gilmore, W.; Correale, J.; Weiner, LP. Coronavirus induction of class I major histocompatibility complex expression in murine astrocytes is virus strain specific. *J. Exp. Med.* **180:**1013–1023; 1995.

[26] Lavi, E.; Gilden, D. H.; Wrobleska, Z.; Rorke, L. B.; Whitelock, M. Experimental demyelination produced by the A59 strain of mouse hepatitis virus. *Neurology* **34:** 597–603; 1984.

[27] Tsuhako, M. H.; Augusto, O.; Linares, E.; Dagli, M. L. Z.; Pereira, C. A. Association between nitric oxide synthesis and vaccination-acquired resistance to murine hepatitis virus by SPF mice. *Free Radic. Biol. Med.* **41:**1534–1541; 2006.

[28] Coley, S. E.; Lavi, E.; Sawicki, S. G.; Fu, L.; Schelle, B.; Karl, N.; Siddell, S. G.; Thiel, V. Recombinant mouse hepatitis virus strain A59 from cloned, full-length cDNA replicates to high titers in vitro and is fully pathogenic in vivo. *J. Virol.* **79:** 3097–3106; 2005.

[29] Linares, E.; Giorgio, S.; Augusto, O. Inhibition of in vivo leishmanicidal mechanisms by tempol: nitric oxide down-regulation and oxidant scavenging. *Free Radic. Biol. Med.* **44:**1668–1676; 2008.

[30] Berube, G. R.; Powers, M. M.; Clarck, G. Iron hematoxylin chelates. I. The Weil staining bath. *Stain. Technol.* **40:**53–62; 1965.

[31] Fabis, M. J.; Scott, G. S.; Kean, R. B.; Koprowski, H.; Hooper, D. C. Loss of blood–brain barrier integrity in the spinal cord is common to experimental allergic encephalomyelitis in knockout mouse models. *Proc. Natl. Acad. Sci. USA* **104:** 5656–5661; 2009.

[32] Chadi, G.; Rosen, L.; Cintra, A.; Tinner, B.; Zoli, M.; Pettersson, R. F.; Fuxe, K. Corticosterone increases FGF-2 (bFGF) immunoreactivity in the substantia nigra of the rat. *NeuroReport* **4:**783–786; 1993.

[33] Salinovich, O.; Montelano, R. C. Reversible staining and peptide mapping of proteins transferred to nitrocellulose after separation by sodium dodecyl sulfate–polyacrylamide gel electrophoresis. *Anal. Biochem.* **156:**341–347; 1986.

[34] Moreira, C.; Tsuhako, M. H.; de Franco, M. T.; Modolell, M.; Pereira, C. A. Arginine metabolism during macrophage autocrine activation and infection with mouse hepatitis virus 3. *Immunobiology* **209:**585–598; 2004.

[35] Frei, K.; Eugster, H. P.; Bopst, M.; Constantinescu, C. S.; Lavi, E.; Fontana, A. Tumor necrosis factor alpha and lymphotoxin alpha are not required for induction of acute experimental autoimmune encephalomyelitis. *J. Exp. Med.* **185:**2177–2182; 1997.

[36] Tanaka, Y.; Koido, S.; Xia, J.; Ohana, M.; Liu, C.; Cote, G. M.; Sawyer, D. B.; Calderwood, S.; Gong, J. Development of antigen-specific CD8+ CTL in MHC class I-deficient mice through CD4 to CD8 conversion. *J. Immunol* **172:**7848–7858; 2004.

[37] Munder, M.; Eichmann, K.; Moran, J. M.; Centeno, F.; Soler, G.; Modolell, M. Th1/Th2-regulated expression of arginase isoforms in murine macrophages and dendritic cells. *J. Immunol.* **163:**3771–3777; 1999.

[38] Wilcox, C. S.; Pearlman, A. Chemistry and antihypertensive effects of tempol and other nitroxides. *Pharmacol. Rev.* **60:**418–469; 2008.

[39] Hawkins, B. T.; Davis, T. P. The blood–brain barrier/neurovascular unit in health and disease. *Pharmacol. Rev.* **57:**173–185; 2005.

[40] Victor, V. M.; Rocha, M.; De la Fuente, M. Immune cells: free radicals and antioxidants in sepsis. *Int. Immunopharmacol.* **4:**327–347; 2004.

[41] Nencioni, L.; Luvara, A.; Aquilano, K.; Ciriolo, M. R.; Cozzolino, F.; Rotilio, G.; Garaci, E.; Palamara, A. T. Influenza A virus replication is dependent on an antioxidant pathway that involves GSH and Bcl-2. *FASEB J.* **17:**758–760; 2003.

[42] Sahaf, B.; Heydari, K.; Herzenberg, L. A.; Herzenberg, L. A. The extracellular microenvironment plays a key role in regulating the redox status of cell surface proteins in HIV-infected subjects. *Arch. Biochem. Biophys.* **434:**26–32; 2005.

[43] Carta, S.; Catellani, P.; Delfino, L.; Tassi, S.; Vené, R.; Rubatlelli, A. DAMPS and inflammatory processes: the role of redox in the different outcomes. *J. Leukocyte Biol.* **86:**549–555; 2009.

[44] Cuzzocrea, S.; Pisano, B.; Dugo, L.; Ianaro, A.; Patel, N. S.; Caputi, A. P.; Thiemermann, C. Tempol reduces the activation of nuclear factor-kappaB in acute inflammation. *Free Radic. Res.* **38:**813–819; 2004.

[45] Akaike, T.; Maeda, H. Nitric oxide and virus infection. *Immunology* **101:**300–308; 2000.

[46] Akaike, T.; Fujii, S.; Kato, A.; Yoshitake, J.; Miyamoto, Y.; Sawa, T.; Okamoto, S.; Suga, M.; Asakawa, M.; Nagai, Y.; Maeda, H. Viral mutation accelerated by nitric oxide production during infection in vivo. *FASEB J.* **14:**1447–1454; 2000.

[47] Linares, E.; Giorgio, S.; Mortara, R. A.; Santos, C. X.; Yamada, A. T.; Augusto, O. Role of peroxynitrite in macrophage microbicidal mechanisms in vivo revealed by protein nitration and hydroxylation. *Free Radic. Biol. Med.* **30:**1234–1242; 2001.

[48] Bonini, M.; Mason, R. P.; Augusto, O. The mechanism by which 4-hydroxy-2,2,6,6-tetramethylpiperidene-1-oxyl (tempol) diverts peroxynitrite decomposition from nitrating to nitrosating species. *Chem. Res. Toxicol.* **15:**506–511; 2002.

[49] Fernandes, D. C.; Medinas, D. B.; Alves, M. J.; Augusto, O. Tempol diverts peroxynitrite/carbon dioxide reactivity toward albumin and cells from protein-tyrosine nitration to protein-cysteine nitrosation. *Free Radic. Biol. Med.* **38:** 189–200; 2005.

[50] Chen, B. P.; Lane, T. E. Lack of nitric oxide synthase type 2 (NOS2) results in reduced neuronal apoptosis and mortality following mouse hepatitis virus infection of the central nervous system. *J. Neurovirol.* **8:**58–63; 2002.

[51] Hooper, D. C.; Spitsin, S.; Kean, R. B.; Champion, J. M.; Dickson, G. M.; Chaudhry, I.; Koprowski, H. Uric acid, a natural scavenger of peroxynitrite, in experimental allergic encephalomyelitis and multiple sclerosis. *Proc. Natl. Acad. Sci. USA* **95:** 675–680; 1998.

[52] Hooper, D. C.; Scott, G. S.; Zborek, A.; Mikheeva, T.; Kean, R. B.; Koprowski, H.; Spitsin, S. V. Uric acid, a peroxynitrite scavenger, inhibits CNS inflammation, blood–CNS barrier permeability changes, and tissue damage in a mouse model of multiple sclerosis. *FASEB J.* **14:**691–698; 2000.

[53] Augusto, O.; Queiroz, R. F.; Vaz, S. M.; Malvezzi, A.; T-do Amaral, A.; Jordão, A. K.; Cunha, A. C.; Ferreira, V. F. Inhibition of the chlorinating activity of myeloperoxidase by nitroxides. 6th International Human Peroxidase Meeting, Chapel Hill, North Caroline, April 19–22, 2009.

[54] Nagra, R. M.; Becher, B.; Tourtellotte, W. W.; Antel, J. P.; Gold, D.; Paladino, T.; Smith, R. A.; Nelson, J. R.; Reynolds, W. F. Immunohistochemical and genetic evidence of myeloperoxidase involvement in multiple sclerosis. *J. Neuroimmunol.* **78:**97–107; 1997.

[55] Chen, J. W.; Breckwoldt, M. O.; Aikawa, E.; Chiang, G.; Weissleder, R. Myeloperoxidase-targeted imaging of active inflammatory lesions in murine experimental autoimmune encephalomyelitis. *Brain* **131:**1123–1133; 2008.